Connecting Dissipation and Phase Slips in a Josephson Junction between Fermionic Superfluids

A. Burchianti,[1,2] F. Scazza,[1,2,*] A. Amico,[2] G. Valtolina,[1,2,†] J. A. Seman,[3] C. Fort,[1,2] M. Zaccanti,[1,2] M. Inguscio,[1,2] and G. Roati[1,2]

[1]*Istituto Nazionale di Ottica del Consiglio Nazionale delle Ricerche (INO-CNR), 50019 Sesto Fiorentino, Italy*
[2]*LENS and Dipartimento di Fisica e Astronomia, Università di Firenze, 50019 Sesto Fiorentino, Italy*
[3]*Instituto de Fisica, Universidad Nacional Autónoma de México, 01000 Ciudad de México, Mexico*

(Received 17 July 2017; published 12 January 2018)

We study the emergence of dissipation in an atomic Josephson junction between weakly coupled superfluid Fermi gases. We find that vortex-induced phase slippage is the dominant microscopic source of dissipation across the Bose-Einstein condensate–Bardeen-Cooper-Schrieffer crossover. We explore different dynamical regimes by tuning the bias chemical potential between the two superfluid reservoirs. For small excitations, we observe dissipation and phase coherence to coexist, with a resistive current followed by well-defined Josephson oscillations. We link the junction transport properties to the phase-slippage mechanism, finding that vortex nucleation is primarily responsible for the observed trends of conductance and critical current. For large excitations, we observe the irreversible loss of coherence between the two superfluids, and transport cannot be described only within an uncorrelated phase-slip picture. Our findings open new directions for investigating the interplay between dissipative and superfluid transport in strongly correlated Fermi systems, and general concepts in out-of-equilibrium quantum systems.

DOI: 10.1103/PhysRevLett.120.025302

The frictionless flow of particles in superfluids and superconductors is a direct manifestation of macroscopic quantum phase coherence. But such systems, in certain conditions, exhibit a nonzero resistivity stemming from dissipative microscopic processes [1–4]. In particular, when superfluids flow through constrictions or channels, the maximum flow is limited by the stochastic nucleation of vortices [4,5]. Vortices traversing the channel cause the phase to slip and remove energy from the superflow, which ceases to be dissipationless [4,6,7]. Phase slips represent the fundamental dissipation mechanism in superfluid helium [4,6,7], and play also an important role for the resistivity of thin superconducting wires and two-dimensional films [3,8–10]. Understanding and controlling dissipation in superfluids is crucial for developing novel quantum devices with ultimate sensitivity [11,12]. In this context, ultracold atomic gases in tailored optical potentials have emerged as a powerful platform [13]. Dissipative dynamics has been observed in Bose-Einstein condensates [14–20], and in superfluid Fermi gases in the presence of either weak obstacles [21–23] or bosonic counterflow [24,25]. Recently, quantum transport through weak links connecting two strongly interacting fermionic superfluids has also been realized, observing different dissipation mechanisms akin to those typical of solid-state devices [26–28]. In particular, for a planar Josephson junction, we revealed the onset of vortex-induced dissipation upon reducing the coupling between the reservoirs [28].

In this work, we demonstrate the direct connection between phase slips and dissipative transport across a Josephson junction between atomic superfluids throughout the Bose-Einstein condensate (BEC)–Bardeen-Cooper-Schrieffer (BCS) crossover. Notwithstanding the different nature of the superfluids herein investigated, we find that phase slippage is the dominant mechanism fostering dissipation of the superfluid energy. We directly detect phase-slip events, emerging as vortex excitations created within the junction and shed into the bulk, and we show the link between the phase-slippage rate and the chemical potential difference across the junction. In the regime of low phase-slippage rate, when few excitations are nucleated, the system exhibits a transient resistive current followed by Josephson plasma oscillations. For larger initial excitations, instead, strong dissipation irreversibly suppresses the Josephson coupling across the junction. We fully characterize the junction by extracting the conductance G and the critical current I_c through a resistively shunted junction model, similar to that used for ordinary superconducting junctions [1,2]. We find G to depend linearly on the superfluid density in the weak-link region, whereas I_c is bounded by the value of the local Landau critical velocity. Our observations deviate from the behavior of typical superconducting junctions [1,2] or unitary superfluids connected by a quantum point contact [27], where dissipation is governed by pair-breaking effects that hinder phase coherence.

We produce fermionic superfluids of $N \simeq 10^5$ atom pairs, cooling a balanced mixture of the two lowest spin states of ^{6}Li to $T/T_F \simeq 0.1$ [29,30]. Here, T_F is the Fermi temperature, $k_B T_F = E_F = \hbar(6N\omega_x\omega_y\omega_z)^{1/3}$, where k_B and $\hbar = h/(2\pi)$ are the Boltzmann and reduced Planck constants,

and $(\omega_x, \omega_y, \omega_z) \simeq 2\pi \times (14, 140, 160)$ Hz are the trapping frequencies. Interactions are parametrized by $1/(k_F a)$, where a is the s-wave scattering length and k_F is the Fermi wave vector defined by $E_F = \hbar^2 k_F^2/(2m)$, with m being the ^{6}Li atomic mass. The scattering length between the two spin states is adjusted via a broad Feshbach resonance located at 832 G [37]. Hereafter, we focus on three distinct regimes of superfluidity: (i) a molecular BEC at $1/(k_F a) \simeq 4.6$, (ii) a unitary superfluid at $1/(k_F a) \simeq 0.05$, and (iii) a BCS superfluid at $1/(k_F a) \simeq -0.6$. We realize the atomic Josephson junction by splitting the superfluid into two weakly coupled reservoirs using a thin Gaussian optical barrier of variable height V_0 and $1/e^2$ width $w \simeq 2$ μm, few times wider than the superfluid coherence length across the BEC-BCS crossover [28,30]. The dynamics is described by the relative population imbalance $z = (N_R - N_L)/N$, corresponding to a chemical potential difference $\Delta\mu = \mu_R - \mu_L$ across the junction, and the relative phase $\varphi = \varphi_L - \varphi_R$ between the two reservoirs, where N_R (N_L) and φ_R (φ_L) are the pair population and phase of the right (left) reservoir, respectively [see Fig. 1(a)]. Experimentally, we monitor the relative population imbalance and phase evolutions by absorption imaging of the *in situ* density and of the interfering reservoirs during a time-of-flight expansion from the trap, respectively [28].

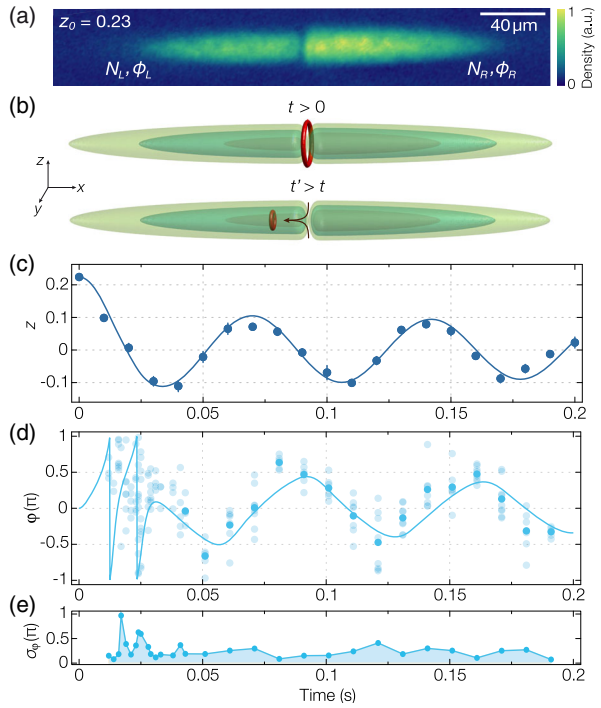

FIG. 1. (a) *In situ* density profile of an atomic superfluid bisected by a thin barrier with $z_0 \simeq 0.23$. (b) Sketch of a phase-slip event: a vortex ring is created within the junction at time t, and it subsequently penetrates into the superfluid bulk after shrinking. (c),(d) Typical population imbalance z and relative phase φ evolutions for a molecular BEC at $1/(k_F a) = 4.6$ and $V_0/\mu = 0.7$. Both solid curves are obtained by a single fit of the measured $z(t)$ with the solution of a RSJ-like circuit model (see text). Error bars in panel (c) denote standard errors over at least five independent measurements, while light (dark) circles in panel (d) represent single (averaged) experimental realizations. (e) Standard deviation of the measured φ. The two peaks at short times are associated with stochastic phase-slip events, where shot-to-shot fluctuations are maximized.

For barrier strengths $V_0 \sim \mu$, the system dynamics is determined essentially by the competition between the Josephson tunneling and charging energy [38–40]. When the tunneling dominates, for small initial excitations, z and φ undergo Josephson plasma oscillations. In the opposite limit of large $\Delta\mu_0$ and in the absence of dissipation, the atomic system is expected to enter the macroscopic self-trapping state, where a linear increase of φ drives small-amplitude oscillations of z around a nonzero value at a frequency $\sim\Delta\mu_0/\hbar$ [38,39,41–44]. To explore the latter regime, we prepare a tunable initial imbalance z_0, corresponding to $\Delta\mu_0/\mu \leq 0.4$, with μ denoting the bulk chemical potential at equilibrium. By lowering the barrier height to the target value V_0 at time $t = 0$, we induce a current $I = \dot{k}$, where $k = zN/2$ [see Fig. 1(a) and Ref. [30] for details]. In Figs. 1(c) and 1(d), $z(t)$ and $\varphi(t)$ are displayed for a molecular BEC with $z_0 \simeq 0.23$ and $V_0/\mu \simeq 0.7$. We observe that z displays an initial decay alongside a fast variation of φ in the range $(-\pi, \pi)$. Thereafter, both $z(t)$ and $\varphi(t)$ oscillate around zero at the Josephson plasma frequency $\omega < \omega_x$ with a relative phase shift of about $\pi/2$. A similar behavior is observed in all explored regimes of superfluidity, as shown in Figs. 2(a)–2(c), where $z(t)$ is compared for BEC, unitary, and BCS superfluids with $z_0 \simeq 0.2$ and $V_0/\mu \simeq 1$. While the observed initial variation of φ is consistent with a running-phase evolution, the irreversible decay of z reflects the instability of the macroscopic self-trapping state [39–41,45]. This highlights the presence of dissipation mechanisms, which could stem from either thermal [14] or collective excitations [28], which however do not destroy the coherent coupling across the junction, as demonstrated by the Josephson dynamics emerging after dissipation. The combination of running-phase evolution and dissipative flow, closely resembling the dynamics of strongly coupled superfluid ^{4}He reservoirs at $T < T_\lambda$ [12], suggests the occurrence of stochastic phase-slip events [see Fig. 1(b)]. This is also supported by the significant fluctuations of φ detected at short times [see Fig. 1(e)].

We gain further insight into the microscopic origin of dissipation by imaging the atomic cloud in time-of-flight after adiabatically removing the barrier [28,30]. We observe the initial drop of z to be accompanied by the presence of vortex defects in the superfluid bulk, detected as local density depletions predominantly located within the reservoir at lower initial chemical potential [see the insets of Figs. 2(d)–2(f)]. In Figs. 2(d)–2(f), we show the time evolution of the mean vortex count $\langle N_v \rangle$ extracted from typically 15 time-of-flight images, acquired in the same

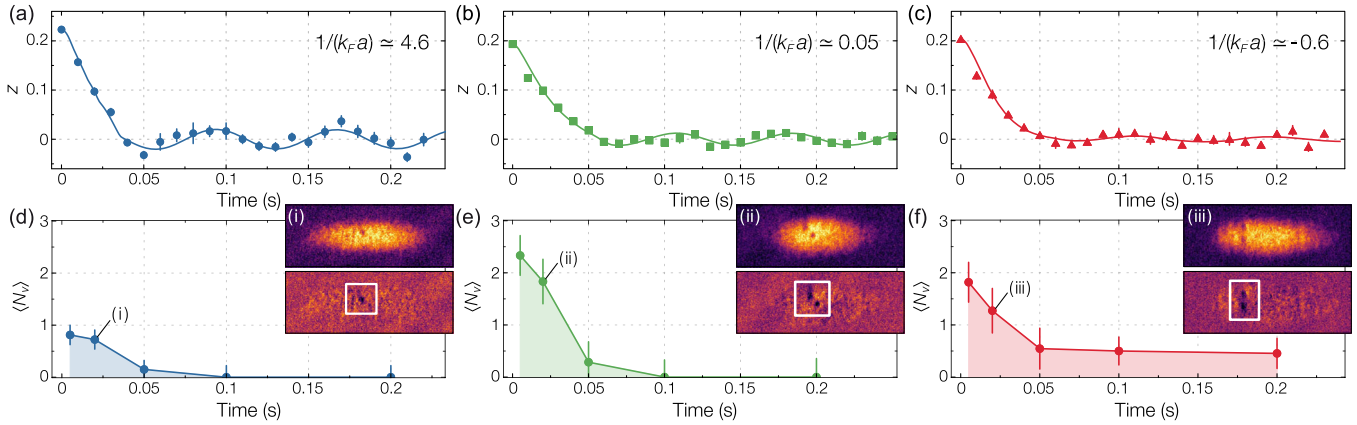

FIG. 2. (a)–(c) Evolution of the relative population imbalance with $z_0 \simeq 0.2$ for (a) a molecular BEC at $V_0/\mu \simeq 1$, (b) a unitary Fermi gas at $V_0/\mu \simeq 0.9$, and (c) a BCS superfluid at $V_0/\mu \simeq 0.9$. Solid lines are fitted to the data with the solution of the circuital model described in the text. Error bars denote standard errors over at least five measurements. (d)–(f) Evolution of average vortex counts $\langle N_v \rangle$ for the same experimental conditions as in panels (a)–(c). The error bars are estimated as $\sqrt{\sigma_{Nv}^2 + 1/Z}$, with σ_{Nv} the standard deviation of the mean and Z the number of experimental measurements. The insets (i)–(iii) show typical time-of-flight images after 20 ms of evolution, where vortex defects are clearly visible. Residual images are also displayed, obtained by subtracting the density distribution of a cloud without excitations.

experimental conditions as in Figs. 2(a)–2(c). In all explored interaction regimes, $\langle N_v \rangle$ is found to decay within the same time scale as z. Such a correlated trend of $z(t)$ and $\langle N_v \rangle(t)$ strongly supports the scenario of dissipation driven by vortex-induced phase-slip events, where the vortex nucleation rate γ, i.e., the phase-slip rate, follows the Josephson-Anderson relation $\gamma \simeq \dot{\varphi}/(2\pi) = \Delta\mu/h$ [6,7]. Accordingly, for a given z_0, $\langle N_v \rangle$ becomes larger when moving from the BEC to the crossover regime, reflecting the increase of $\Delta\mu_0$. Once $z(t)$ has dropped below a critical value, the vortex nucleation rate is strongly reduced, so that $\langle N_v \rangle$ remains low and pure Josephson dynamics is established. $\langle N_v \rangle$ is also determined by the vortex lifetime, which depends on the interaction strength and is limited by vortex decay into soundlike excitations, favored by the density kink at the barrier position [30,46,47]. Although sound waves must ultimately dissipate into heat, we do not observe any related appreciable reduction of the condensed fraction within the measurement time scale [30].

Our observations agree with simulations of weakly linked three-dimensional bosonic superfluids, showing that phase slippage typically arises from vortex rings nucleated within the barrier at the edge of the atomic cloud, which shrink and cross the junction region perpendicularly to the flow [see Fig. 1(b)] [48–50]. We confirm this scenario by performing numerical simulations in the BEC and unitary regimes with the zero-temperature extended Thomas-Fermi model (ETFM), based on a generalized Gross-Pitaevskii equation for the pair's wave function including the chemical potential from quantum Monte Carlo calculations across the entire crossover [30,51]. The simulations correctly capture the decay of z due to vortex shedding into the bulk, which is favored by the multimode character of our junction [30,47]. Experimentally, we observe defects predominantly oriented along the tighter confining trap axis, i.e., the imaging line of sight [see Figs. 2(d)–2(f)]. This is consistent with the instability of vortex rings towards breaking up into vortex lines in a radially asymmetric trap with $\omega_y < \omega_z$ [52], assisted also by the slow barrier removal prior to imaging [30,47].

To quantitatively characterize the transport through the junction, we model it with an equivalent circuit made of three parallel elements: a Josephson weak link with a current-phase relation $I_J = -I_c \sin(\varphi)$, a shunt resistance R, and a series LC [20,30]. In this way, we extract the conductance $G = R^{-1}$ and critical current I_c. The use of this model is justified, as we find the dissipative current to be Ohmic with a linear current-bias relation [30]. This approach is equivalent to the resistively shunted junction (RSJ) model [1,53,54], and it incorporates both a Josephson and a resistive current $I_R = -G\Delta\mu$, where the resistance R can account for various dissipation mechanisms. For superconducting junctions, these typically involve the breaking of Cooper pairs [1,55]. Here, instead, we argue that resistivity originates from vortex-induced phase slippage rather than from unpaired fermions. The measured $z(t)$ is well fitted by the numerical solution of the model, where R and I_c are left as free parameters (see the solid lines in Figs. 1, 3, and 4) [30]. For initial bias potentials $\Delta\mu_0/\mu$ between 0.05 and 0.2, and barrier heights ranging from $V_0/\mu \sim 0.6$ to 1.5, we find that G and I_c do not depend appreciably upon $\Delta\mu_0$ at a given V_0/μ. This is expected for phase-slip-driven dissipation [7,18], in a regime where only few, uncorrelated topological excitations are nucleated into the superfluid [see Figs. 2(d)–2(f)]. For the largest values of V_0, where I_c is strongly reduced [28] and Josephson oscillations are not experimentally resolved, G is extracted using a simple RC circuit model. To directly connect the measured conductances with the phase-slippage mechanism,

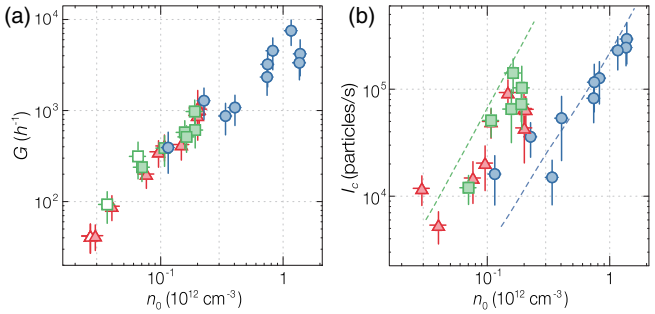

FIG. 3. (a) Conductance G and (b) critical current I_c as a function of the central pair-density n_0 inside the barrier for BEC (blue circles), unitary (green squares), and BCS (red triangles) superfluids. For filled (empty) symbols, G is obtained through the RSJ-like (RC) circuit model (see text). The dashed lines in panel (b) represent the calculated upper bound I_{c0} [30], shown for comparison for BEC (blue) and unitary (green) superfluids. In both panels, horizontal error bars account for the typical 20% uncertainty on atom number, while vertical ones combine this with fitting standard errors.

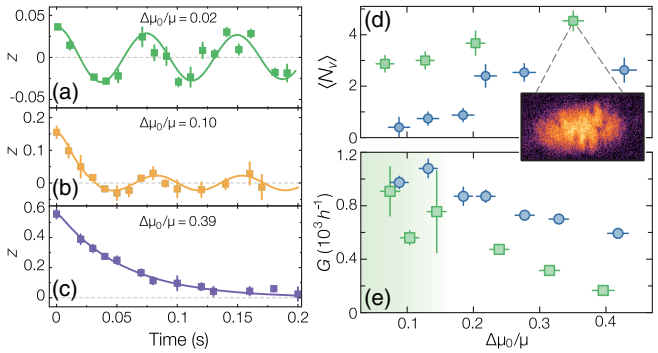

FIG. 4. (a)–(c) Crossover from Josephson to purely dissipative dynamics in a unitary superfluid at $V_0/\mu \simeq 0.9$. The initial bias potentials $\Delta\mu_0/\mu$ are (a) 0.02, (b) 0.10, and (c) 0.39. (d) Average vortex counts $\langle N_v \rangle$ and (e) conductance G as a function of $\Delta\mu_0/\mu$ for BEC superfluids at $V_0/\mu \simeq 1.3$ (blue circles) and unitary superfluids at $V_0/\mu \simeq 0.9$ (green squares). The central density n_0 is about 3 times larger for BECs with respect to unitary gases. The green shaded region indicates the range of $\Delta\mu_0/\mu$ where $I_c > 0$ at unitarity. Vertical error bars are computed as described in the caption of Figs. 2 and 3, while horizontal ones result from the experimental uncertainty on z_0, which is typically of $\pm 2\%$. Inset: time-of-flight image of an expanding unitary superfluid for $\Delta\mu_0/\mu \simeq 0.35$, where several vortex defects are visible.

we express the resistive current as $I_R \propto N_{\mathrm{ex}}\gamma$, where N_{ex} is the number of particles participating in each excitation [18]. For phase slippage, $\gamma \simeq \Delta\mu/h$, which yields $G = -I_R/\Delta\mu \propto N_{\mathrm{ex}}/h$. Therefore, we expect $G \propto n_0$, where n_0 is the central density inside the barrier where the excitations form. Even though we are not able to directly measure n_0, due to the 1.5 μm imaging resolution and to light-induced atom diffusion during the imaging pulse, we efficiently estimate $n_0 = n_0(V_0/\mu)$ by the equilibrium solution of the extended Thomas-Fermi model [30]. In this way, we can relate the values G and I_c extracted for each value of V_0/μ to n_0.

Figure 3(a) displays the conductance G in units of h^{-1} as a function of n_0 for BEC, unitary, and BCS superfluids. To test the linearity of the measured G, we fit the experimental data with a power law, $G \propto n_0^{\alpha}$. For BEC and unitary regimes, we indeed find $\alpha = 1.0(3)$ and $\alpha = 1.1(2)$, respectively. For BCS superfluids, we instead obtain $\alpha = 1.5(2)$. This nonlinearity may stem from the limited accuracy of our n_0 estimate in the BCS regime and from additional dissipation sources such as single-particle excitations. Importantly, we observe approximately matching conductances at fixed n_0 regardless of the specific nature of the superfluid, evidencing the dominant role of phase slippage. The large values of G highlight the composite bosonic nature of the tunneling particles carrying the current. Furthermore, our findings elucidate the origin of the finite resistance measured for unitary superfluids connected via a quasi-two-dimensional channel [26]. In Fig. 3(b), the extracted critical current I_c is presented as a function of n_0 in the different interaction regimes. In contrast to G, we find that I_c depends on the nature of the condensate across the BEC-BCS crossover. Resonant superfluids display the largest I_c at a given n_0, confirming their enhanced robustness [21,23,28], also in the presence of dissipation. I_c is expected to be associated with the critical velocity for vortex nucleation at the superfluid surface inside the barrier [22,56]. For BEC and unitary superfluids, the latter is predicted to be lower than the local sound speed c [22,49,56], yielding an upper bound $I_{c0} = cn_{0x}$, where n_{0x} is the radially integrated central density [30]. The experimental data approach the calculated I_{c0}, with trends in qualitative agreement [see the dashed lines in Fig. 3(b)]. Even though c increases moving towards the BCS limit, the measured I_c for BCS superfluids is not larger than at unitarity, evidencing the decrease of the (Landau) critical velocity for vortex nucleation, which becomes bounded by the fermionic excitation branch [41,56]. This is consistent with the drop of Josephson energy $E_J \propto I_c$ observed for a BCS superfluid in the tunneling regime, where such an effect is associated with condensate depletion [28].

For $\Delta\mu_0/\mu \gtrsim 0.2$ the junction enters a qualitatively different regime, where transport properties depend on $\Delta\mu_0$. In Figs. 4(a)–4(c) typical evolutions $z(t)$ are shown for unitary gases at three different values of $\Delta\mu_0/\mu$ with $V_0/\mu \simeq 0.9$. By increasing $\Delta\mu_0/\mu$, we observe the gradual loss of the Josephson oscillation visibility, with the onset of purely dissipative transport around $\Delta\mu_0/\mu \approx 0.2$. We connect the resistance with vortex nucleation by measuring $\langle N_v \rangle(t)$ at varying $\Delta\mu_0/\mu$, for a unitary Fermi gas and BEC at $V_0/\mu \simeq 0.9$ and $V_0/\mu \simeq 1.3$, respectively. The results are displayed in Fig. 4(d). In Fig. 4(d) we present also the measured G as a function of $\Delta\mu_0/\mu$. In both cases, G decreases for $\Delta\mu_0/\mu \gtrsim 0.2$. The increase of the bias potential leads to the increase of γ and therefore of $\langle N_v \rangle$. However, the decrease of G is unexpected in a linear, uncorrelated phase-slip picture, where $\dot{\varphi} \propto \Delta\mu$: the observed behavior implies that our system cannot support

an arbitrary large nucleation rate. Moreover, the disappearance of Josephson oscillations suggests that the coherent coupling between the reservoirs is irreversibly affected by phase-slip proliferation [4]. The presence of several vortices interacting near the barrier may create a local turbulent pad region [57,58], where the superfluid density is locally suppressed. On the other hand, the accumulation of vortices may locally scramble the relative phase, thereby suppressing the critical current akin to thermal fluctuations in superconducting junctions [2]. The saturation of the vortex production rate may arise from vortex reconnections and interactions [58,59]. Our observations cannot be ascribed to an increase of the sample temperature, since the condensed fraction in the BEC regime remains above 0.7, limited only by the intrinsic lifetime of the gas [30].

In conclusion, our findings extend the vortex-induced phase-slippage picture of dissipation typical of liquid ^{4}He to weakly coupled, strongly correlated atomic Fermi gases. We have found that in BEC-BCS crossover superfluids phase coherence can coexist with dissipation, afforded by topological excitations that, not depleting the condensate, do not cause the breakdown of Josephson dynamics. Future experiments will further explore the far-from-equilibrium regime, addressing the role of vortex proliferation and mutual interactions. Moreover, it will be interesting to investigate the effect of fluctuations around the superfluid critical temperature [60]. Our system offers a promising platform for exploring dissipative fermionic transport phenomena like quantum turbulence [58] and dissipation-driven quantum phase transitions [10,61,62].

We acknowledge inspiring discussions with F. Dalfovo, T. Giamarchi, F. Piazza, N. Proukakis, A. Smerzi, A. Trombettoni, and K. Xhani. We especially acknowledge the LENS Quantum Gases group. This work was supported by the ERC through Grant No. 307032 QuFerm2D and by the Marie Skłodowska-Curie programme (Grant No. 705269 to F. S.). J. A. S. acknowledges supporting grants from Universidad Nacional Autónoma de México–Dirección General de Asuntos del Personal Académico/Programa de Apoyo a Proyectos de Investigación e Innovación Tecnológica IA101716 and Consejo Nacional de Ciencia y Tecnología (CONACyT) LN-271322.

*Corresponding author.
scazza@lens.unifi.it
†Present address: JILA, University of Colorado, Boulder, Colarado 80309, USA.

[1] A. Barone and G. Paternò, *Physics and Applications of the Josephson Effect* (Wiley, New York, 1982).
[2] M. Tinkham, *Introduction to Superconductivity*, 2nd ed. (McGraw-Hill, New York, 1996).
[3] B. I. Halperin, G. Refael, and E. Demler, Int. J. Mod. Phys. B **24**, 4039 (2010).
[4] E. Varoquaux, Rev. Mod. Phys. **87**, 803 (2015).
[5] R. P. Feynman, in *Progress in Low Temperature Physics*, edited by C. J. Gorter (North-Holland, Amsterdam, 1955).
[6] P. W. Anderson, Rev. Mod. Phys. **38**, 298 (1966).
[7] O. Avenel and E. Varoquaux, Phys. Rev. Lett. **55**, 2704 (1985).
[8] J. S. Langer and V. Ambegaokar, Phys. Rev. **164**, 498 (1967).
[9] A. Bezryadin, C. N. Lau, and M. Tinkham, Nature (London) **404**, 971 (2000).
[10] Y. Chen, Y.-H. Lin, S. D. Snyder, A. M. Goldman, and A. Kamenev, Nat. Phys. **10**, 567 (2014).
[11] J. Clarke and A. I. Braginski, *The SQUID Handbook* (Wiley-VCH, Weinheim, 2004).
[12] Y. Sato and R. E. Packard, Rep. Prog. Phys. **75**, 016401 (2012).
[13] C.-C. Chien, S. Peotta, and M. Di Ventra, Nat. Phys. **11**, 998 (2015).
[14] S. Levy, E. Lahoud, I. Shomroni, and J. Steinhauer, Nature (London) **449**, 579 (2007).
[15] D. McKay, M. White, M. Pasienski, and B. DeMarco, Nature (London) **453**, 76 (2008).
[16] S. Moulder, S. Beattie, R. P. Smith, N. Tammuz, and Z. Hadzibabic, Phys. Rev. A **86**, 013629 (2012).
[17] K. C. Wright, R. B. Blakestad, C. J. Lobb, W. D. Phillips, and G. K. Campbell, Phys. Rev. Lett. **110**, 025302 (2013).
[18] F. Jendrzejewski, S. Eckel, N. Murray, C. Lanier, M. Edwards, C. J. Lobb, and G. K. Campbell, Phys. Rev. Lett. **113**, 045305 (2014).
[19] L. Tanzi, S. Scaffidi Abbate, F. Cataldini, L. Gori, E. Lucioni, M. Inguscio, G. Modugno, and C. D'Errico, Sci. Rep. **6**, 25965 (2016).
[20] S. Eckel, J. G. Lee, F. Jendrzejewski, C. J. Lobb, G. K. Campbell, and W. T. Hill, III, Phys. Rev. A **93**, 063619 (2016).
[21] D. E. Miller, J. K. Chin, C. A. Stan, Y. Liu, W. Setiawan, C. Sanner, and W. Ketterle, Phys. Rev. Lett. **99**, 070402 (2007).
[22] G. Watanabe, F. Dalfovo, F. Piazza, L. P. Pitaevskii, and S. Stringari, Phys. Rev. A **80**, 053602 (2009).
[23] W. Weimer, K. Morgener, V. P. Singh, J. Siegl, K. Hueck, N. Luick, L. Mathey, and H. Moritz, Phys. Rev. Lett. **114**, 095301 (2015).
[24] M. Delehaye, S. Laurent, I. Ferrier-Barbut, S.Jin, F. Chevy, and C. Salomon, Phys. Rev. Lett. **115**, 265303 (2015).
[25] Y. Castin, I. Ferrier-Barbut, and C. Salomon, C.R. Phys. **16**, 241 (2015).
[26] D. Stadler, S. Krinner, J. Meineke, J. P. Brantut, and T. Esslinger, Nature (London) **491**, 736 (2012).
[27] D. Husmann, S. Uchino, S. Krinner, M. Lebrat, T. Giamarchi, T. Esslinger, and J. P. Brantut, Science **350**, 1498 (2015).
[28] G. Valtolina, A. Burchianti, A. Amico, E. Neri, K. Xhani, J. A. Seman, A. Trombettoni, A. Smerzi, M. Zaccanti, M. Inguscio, and G. Roati, Science **350**, 1505 (2015).
[29] A. Burchianti, G. Valtolina, J. A. Seman, E. Pace, M. De Pas, M. Inguscio, M. Zaccanti, and G. Roati, Phys. Rev. A **90**, 043408 (2014).
[30] See Supplemental Material at http://link.aps.org/supplemental/10.1103/PhysRevLett.120.025302 for details on the experimental procedures, and the theoretical methods and simulations, which includes Refs. [31–36].

[31] M. J. H. Ku, W. Ji, B. Mukherjee, E. Guardado-Sanchez, L. W. Cheuk, T. Yefsah, and M. W. Zwierlein, Phys. Rev. Lett. **113**, 065301 (2014).
[32] J. G. Lee, B. J. McIlvain, C. J. Lobb, and W. T. Hill, III, Sci. Rep. **3**, 1034 (2013).
[33] M. J. H. Ku, A. T. Sommer, L. W. Cheuk, and M. W. Zwierlein, Science **335**, 563 (2012).
[34] S. Gandolfi, K. E. Schmidt, and J. Carlson, Phys. Rev. A **83**, 041601(R) (2011).
[35] E. Zaremba, Phys. Rev. A **57**, 518 (1998).
[36] P. Capuzzi, P. Vignolo, F. Federici, and M. P. Tosi, Phys. Rev. A **73**, 021603(R) (2006).
[37] G. Zürn, T. Lompe, A. N. Wenz, S. Jochim, P. S. Julienne, and J. M. Hutson, Phys. Rev. Lett. **110**, 135301 (2013).
[38] A. Smerzi, S. Fantoni, S. Giovanazzi, and S. R. Shenoy, Phys. Rev. Lett. **79**, 4950 (1997).
[39] I. Zapata, F. Sols, and A. J. Leggett, Phys. Rev. A **57**, R28(R) (1998).
[40] F. Meier and W. Zwerger, Phys. Rev. A **64**, 033610 (2001).
[41] P. Zou and F. Dalfovo, J. Low Temp. Phys. **177**, 240 (2014).
[42] M. Albiez, R. Gati, J. Fölling, S. Hunsmann, M. Cristiani, and M. K. Oberthaler, Phys. Rev. Lett. **95**, 010402 (2005).
[43] M. Abbarchi, A. Amo, V. G. Sala, D. D. Solnyshkov, H. Flayac, L. Ferrier, I. Sagnes, E. Galopin, A. Lematre, G. Malpuech, and J. Bloch, Nat. Phys. **9**, 275 (2013).
[44] G. Spagnolli, G. Semeghini, L. Masi, G. Ferioli, A. Trenkwalder, S. Coop, M. Landini, L. Pezze', G. Modugno, M. Inguscio *et al.*, Phys. Rev. Lett. **118**, 230403 (2017).
[45] J. Ruostekoski and D. F. Walls, Phys. Rev. A **58**, R50 (1998).
[46] K. Suthar, A. Roy, and D. Angom, J. Phys. B **47**, 135301 (2014).
[47] Further theoretical investigations of vortex dynamics at finite temperature are ongoing, in collaboration with Professor N. Proukakis.
[48] F. Piazza, L. A. Collins, and A. Smerzi, New J. Phys. **13**, 043008 (2011).
[49] F. Piazza, L. A. Collins, and A. Smerzi, J. Phys. B **46**, 095302 (2013).
[50] M. Abad, M. Guilleumas, R. Mayol, F. Piazza, D. M. Jezek, and A. Smerzi, Eur. Phys. Lett. **109**, 40005 (2015).
[51] M. McNeil Forbes and R. Sharma, Phys. Rev. A **90**, 043638 (2014).
[52] M. J. H. Ku, B. Mukherjee, T. Yefsah, and M. W. Zwierlein, Phys. Rev. Lett. **116**, 045304 (2016).
[53] W. C. Stewart, Appl. Phys. Lett. **12**, 277 (1968).
[54] D. E. McCumber, J. Appl. Phys. **39**, 3113 (1968).
[55] I. Giaever, Phys. Rev. Lett. **5**, 464 (1960).
[56] A. Spuntarelli, P. Pieri, and G. C. Strinati, Phys. Rev. Lett. **99**, 040401 (2007).
[57] M. C. Tsatsos, P. E. S. Tavares, A. Cidrim, A. R. Fritsch, M. A. Caracanhas, F. E. A. dos Santos, C. F. Barenghi, and V. S. Bagnato, Phys. Rep. **622**, 1 (2016).
[58] A. Bulgac, M. M. Forbes, and G. Wlazlowski, J. Phys. B **50**, 014001 (2017).
[59] S. Serafini, L. Galantucci, E. Iseni, T. Bienaimé, R. N. Bisset, C. F. Barenghi, F. Dalfovo, G. Lamporesi, and G. Ferrari, Phys. Rev. X **7**, 021031 (2017).
[60] B. Liu, H. Zhai, and S. Zhang, Phys. Rev. A **90**, 051602(R) (2014).
[61] A. O. Caldeira and A. J. Leggett, Ann. Phys. (N.Y.) **149**, 374 (1983).
[62] M. P. A. Fisher, Phys. Rev. Lett. **57**, 885 (1986).